Physical and Apparent Arrhenius Constitutive models of a Nb–Ti Microalloyed C–Mn–Al High Strength Steel: A Comparative Study

Hai-lian Wei[1,2] · Hong-bo Pan[3] · Hong-wei Zhou[1,2]

Abstract The flow stress curves of a Nb–Ti microalloyed C–Mn–Al high strength steel were obtained by hot compression experiment with Gleeble-1500 thermal simulator at the temperatures from 900 to 1100 °C and strain rates from 0.01 to 30 s^{-1}. Firstly, strain-compensated physical constitutive models considering the temperature dependence of Young's modulus (E) and austenite self-diffusion coefficient (D) with creep stress exponent 5 and variable stress exponent n' were established, respectively. Secondly, the traditional apparent Arrhenius constitutive model was established to compare the accuracy of the models. The results show that the physical constitutive model with exponent n' has higher accuracy to predict the flow stress of the experimental steel (correlation coefficient $R = 0.992$, average absolute relative error $\delta = 3.83\%$) than the model with exponent 5 (correlation coefficient $R = 0.990$, average absolute relative error $\delta = 10.54\%$). This is because when the stress exponent in the physical constitutive model is 5, it means that the deformation mechanism considered is only slip and climb, and the constitutive model with variable stress exponent n' considers all the deformation mechanisms comprehensively, so the prediction accuracy is higher. The correlation coefficient R of the Arrhenius constitutive model is 0.991, and the average absolute relative error δ is 4.58%. Therefore, the physical constitutive model with exponent n' has the highest prediction accuracy in this study, thus can be an alternative way to predict the flow curves of steels.

1 Introduction

Development of high strength steels with good ductility and toughness has long been pursued in steel industries. As a result, several advanced steels have been introduced, including transformation induced plasticity (TRIP) steels. TRIP steels have excellent mechanical properties, mainly due to the strengthening of martensite and TRIP effect, and have great development potential in the application of automotive structural parts and reinforcements [1]. Conventional TRIP steels were developed based on the C–Mn–Si alloy system. Nowadays, C–Mn–Al–Si or C–Mn–Al based TRIP steels which reduce or remove the harmful effects of Si on galvanizability with good mechanical properties have attracted more and more attention, and a lot of works focused on the characteristics of microstructural development and mechanical behavior of C–Mn–Al–Si or C–Mn–Al based TRIP steels [2–12]. But there are relatively few detailed reports on the hot deformation behavior of such steels.

Constitutive equation, as an important model that describes the relationship between thermodynamic parameters in hot working, plays an important role in the finite

✉ Hai-lian Wei
    whl0403@126.com

1   Key Laboratory of Green Fabrication and Surface Technology of Advanced Metal Materials (Anhui University of Technology), Ministry of Education, Ma'anshan 243002, Anhui, China

2   School of Materials Science and Engineering, Anhui University of Technology, Ma'anshan 243002, Anhui, China

3   Key Laboratory of Metallurgical Emission Reduction and Resources Recycling of Ministry of Education, Ma'anshan, China

element numerical simulation technology and the optimization of forming process parameters. At present, many researches focus on the traditional apparent Arrhenius hyperbolic sine constitutive equation (Eq. (1)) [13–16]. In the Arrhenius constitutive equation, the effects of temperature and strain rate on the hot deformation behavior of materials can be expressed by the Zener–Hollomon parameter Z.

$$Z = \dot{\varepsilon} \exp\left(\frac{Q}{RT}\right) = A[\sinh(\alpha\sigma)]^n \tag{1}$$

where $\dot{\varepsilon}$ is the strain rate, s^{-1}; A, α, n are material constants; R is the gas constant, 8.3145 J mol^{-1} K^{-1}; Q is the hot deformation activation energy, J mol^{-1}; T is the temperature, K; σ is the flow stress, MPa.

The traditional Arrhenius constitutive equation is widely used, but it is considered that the equation generally takes no account of the internal microstructure, leading to apparent rather than actual values in the constants calculated [17–19]. At present, a physical constitutive equation based on creep theory which takes into account the dependence of Young's modulus (E) and austenite's self-diffusion coefficient (D) on temperature with a constant creep stress exponent 5 has attracted more and more attention, as shown in Eq. (2).

$$\dot{\varepsilon}/D(T) = B[\sinh(\alpha'\sigma/E(T))]^5 \tag{2}$$

where α' and B are material constants, $D(T) = D_0\exp(Q_{sd}/(RT))$, D_0 is diffusion constant, Q_{sd} is self-diffusion activation energy, $E(T)$ describes the relationship between Young's modulus and temperature.

Results show that the physical constitutive equation not only has certain physical backgrounds, but also is easier to calculate than the Arrhenius constitutive equation, which can be used to study the hot deformation behavior of vanadium microalloyed steel, 17-4PH stainless steel, 304 stainless steel and 35Mn2 steel [17–22], and it is found that modifying the creep stress exponent 5 to variable stress exponent n' can improve the fitting accuracy of the physical constitutive equation [22]. Further studies show that the strain-compensated physical constitutive equation can predict the hot deformation flow stress curves of C–Mn steel, vanadium microalloyed steel, Ti alloy and Zr alloy accurately [23–26]. However, there is no report on the physical constitutive equation to study the hot deformation behavior of microalloyed C–Mn–Al high strength steel.

In this paper, the physical constitutive equation and the traditional Arrhenius hyperbolic sine constitutive equation are used to study the constitutive relationship of a Nb–Ti microalloyed C–Mn–Al high-strength steel, and a comparative analysis is carried out. The results of this study can provide a simple and effective method in hot working of microalloyed C–Mn–Al high strength steel, and at the same time further enrich the research scope of the physical constitutive equation.

2 Experimental materials and procedures

The chemical composition of the steel used in this investigation is given in Table 1.

The experimental steel was melted by vacuum induction furnace, hot forged and rolled to 20 mm thick plate and then fabricated into Φ8 × 15 mm cylindrical specimen. The austenite single-phase deformation was carried out by uniaxial compression experiment on Gleeble-1500 thermomechanical simulator. Deformation temperatures were 900, 950, 1000, 1050 and 1100 °C, strain rates were 0.01, 0.1, 1, 10 and 30 s^{-1}, and engineering strain was 0.6. The specific hot deformation process is shown in Fig. 1.

3 Results and discussion

3.1 Physical constitutive models

Frost and Ashby [27] established the relationships between the self-diffusion coefficient and Young's modulus as a function of temperature for various materials. Among them, γ-Fe is the material most similar to the experimental steel, so the data of γ-iron can be used and the following expressions are obtained for $D(T)$ and $E(T)$.

$$D(T) = D_0 \exp\left(\frac{-Q}{RT}\right) = 1.8 \times 10^{-5} \exp\left(\frac{-270000}{RT}\right) \tag{3}$$

$$\begin{aligned} E(T) &= E_0\left(1 - \frac{T_M}{G_0}\frac{dG}{dT}\frac{(T-300)}{T_M}\right) \\ &= 2.16 \times 10^5\left(1 - 0.91\frac{(T-300)}{1810}\right) \end{aligned} \tag{4}$$

where E_0 and G_0 represent Young's modulus and shear modulus of the material at 300 K, respectively, T_m is the melting point of the material.

3.1.1 Physical constitutive model with creep stress exponent 5

In Eq. (2), there are two unknown parameters B and α' need to be determined. Mirzadeh et al. [20] proposed a simple linear regression method. In this method, Eqs. (5) and (6) were introduced and peak stress (σ_P) was chosen for analysis.

$$\dot{\varepsilon}/D(T) = B'(\sigma_P/E(T))^{n'_1} \tag{5}$$

Table 1 Chemical composition of the experimental steel (wt%)

| C	Si	Al	Mn	Cr	Mo	B	Ni	Nb	Ti	S	P	N
0.23	< 0.10	1.79	1.50	1.0	0.25	0.006	1.0	0.06	0.025	0.0024	0.0084	0.0019
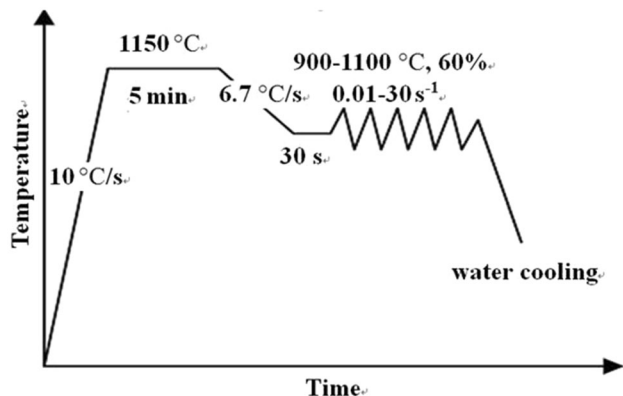
Fig. 1 The hot deformation process

$$\dot{\varepsilon}/D(T) = B'' \exp(\beta'\sigma_P/E(T)) \tag{6}$$

The value of n'_1 and β' can be obtained from the slope of the lines $\ln(\dot{\varepsilon}/D(T)) - \ln(\sigma_p/E(T))$ and $\ln(\dot{\varepsilon}/D(T)) - \sigma_p/E(T)$ plots, respectively. Figure 2 shows both the experimental data and regression results of $\ln(\dot{\varepsilon}/D(T)) - \ln(\sigma_p/E(T))$ (Fig. 2a) and $\ln(\dot{\varepsilon}/D(T)) - \sigma_p/E(T)$ (Fig. 2b) plots. The linear regression of these data results in the value of $n'_1 = 6.9733$, $\beta' = 7362.6853$. The value of α' can be calculated from $\alpha' = \beta'/n'_1 = 1055.836$.

According to Eq. (2), the slope of the plot of $(\dot{\varepsilon}/D(T))^{1/5} - \sinh(\alpha'\sigma_p/E(T))$ by fitting a straight line with an intercept of zero ($y = ax + 0$) was used to obtain the value of $B^{1/5} = 666.6447$ (Fig. 3). Therefore, the
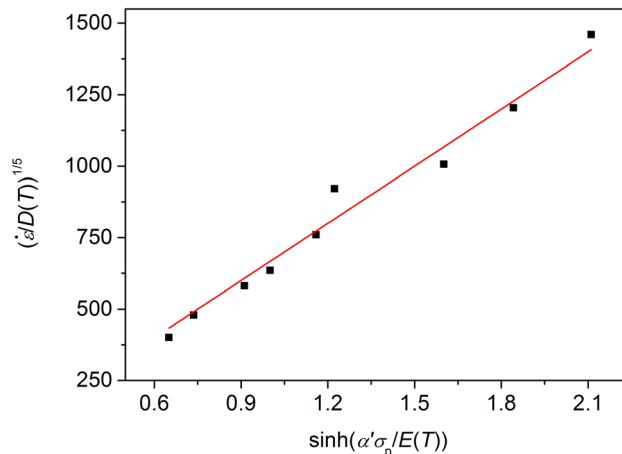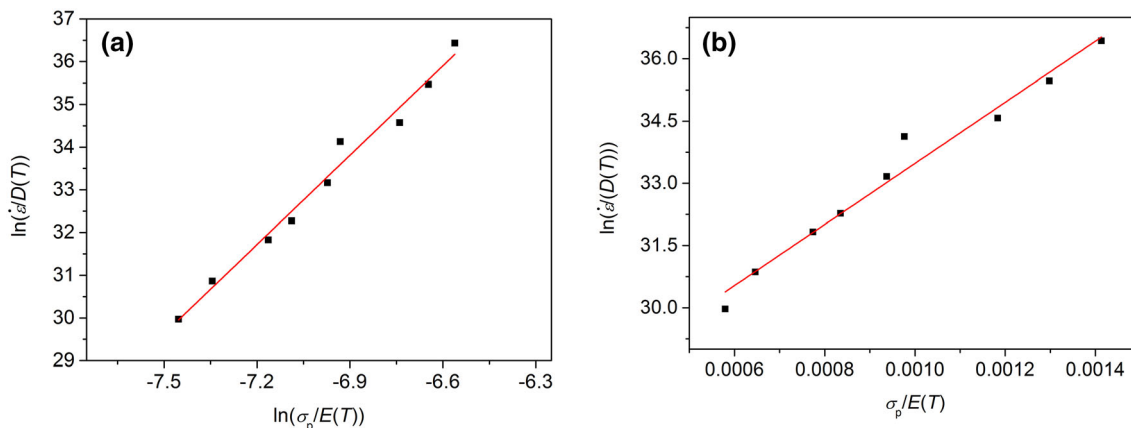

Fig. 3 Relationship between $(\dot{\varepsilon}/D(T))^{1/5}$ and $\sinh(\alpha'\sigma_p/E(T))$

physical constitutive equation of the experimental steel is shown in Eq. (7).

$$\dot{\varepsilon}\exp(270000/RT) = 1.32 \\ \times 10^{14}\left[\sinh\left(1055.836 \times \sigma_p/E(T)\right)\right]^5 \tag{7}$$

Actually, the analysis above only takes into account the peak stress but with no consideration of all strains. Therefore, the strain-compensated physical constitutive model has been established. A series of constitutive equations (Eq. (2)) with different material constants α' and $\ln B$ for different strain values from 0.05 to 0.8 with the interval of 0.05 have been developed. The relationship

Fig. 2 Relationship between **a** $\ln(\dot{\varepsilon}/D(T))$ and $\ln(\sigma_p/E(T))$; **b** $\ln(\dot{\varepsilon}/D(T))$ and $\sigma_p/E(T)$

between α', $\ln B$ and true strain ε can be 5th order polynomial fitted (Eq. (8)) as shown in Fig. 4. The coefficients of the polynomial are provided in Table 2.

$$\alpha'_\varepsilon = \alpha'_0 + \alpha'_1\varepsilon + \alpha'_2\varepsilon^2 + \alpha'_3\varepsilon^3 + \alpha'_4\varepsilon^4 + \alpha'_5\varepsilon^5$$
$$(\ln B)_\varepsilon = B_0 + B_1\varepsilon + B_2\varepsilon^2 + B_3\varepsilon^3 + B_4\varepsilon^4 + B_5\varepsilon^5 \tag{8}$$

By substituting the coefficients listed in Eq. (8) and Table 2 into Eq. (2), the strain-compensated physical constitutive model can be obtained:

$$\sigma = \frac{E(T)}{\alpha'_\varepsilon}\arcsin h\left[\exp\left(\frac{\ln[\dot\varepsilon/D(T)] - (\ln B)_\varepsilon}{5}\right)\right] \tag{9}$$

3.1.2 Physical constitutive model with stress exponent n'

From a metallurgical point of view, considering the self-diffusion activation energy, the creep stress exponent 5 is only valid when the deformation mechanism is controlled by the slip and climb of dislocations [17, 19]. Therefore, the constant creep stress exponent 5 was modified to variable stress exponent n', then the general form of the physical constitutive equation was obtained (Eq. (10)).

$$\dot\varepsilon/D(T) = B'[\sinh(\alpha'\sigma/E(T))]^{n'} \tag{10}$$

In Eq. (10), there are 3 unknowns α', n' and B'. Among them, the calculation of α' in Eq. (2) and Eq. (10) is exactly the same. So $\alpha' = 1055.836$. According to Eq. (10), the slope and intercept of $\ln(\dot\varepsilon/D(T)) - \ln(\sinh(\alpha'\sigma_p/E(T)))$ plot can be used to calculate the value of n' and $\ln B'$, as shown in Fig. 5. Then $n' = 5.28882$, $\ln B' = 32.39515$. Therefore, the physical constitutive equation is shown in Eq. (11).

$$\dot\varepsilon\exp(270000/RT) = 1.17$$
$$\times 10^{14}\left[\sinh\left(1055.836 \times \sigma_p/E(T)\right)\right]^{5.29} \tag{11}$$

In the same way, the strain-compensated physical constitutive model has been established. The relationship between α' in Eq. (10) and ε is also shown in Fig. 4a. The relationship between n', $\ln B'$ and ε was fitted by a 5th order polynomial (Eq. (12)) as shown in Fig. 6, and the coefficients are shown in Table 3.

$$n'_\varepsilon = N'_0 + N'_1\varepsilon + N'_2\varepsilon^2 + N'_3\varepsilon^3 + N'_4\varepsilon^4 + N'_5\varepsilon^5$$
$$(\ln B')_\varepsilon = B'_0 + B'_1\varepsilon + B'_2\varepsilon^2 + B'_3\varepsilon^3 + B'_4\varepsilon^4 + B'_5\varepsilon^5 \tag{12}$$

By substituting the coefficients listed in Eq. (12) and Table 3 into Eq. (10), the strain-compensated physical constitutive model can be obtained:
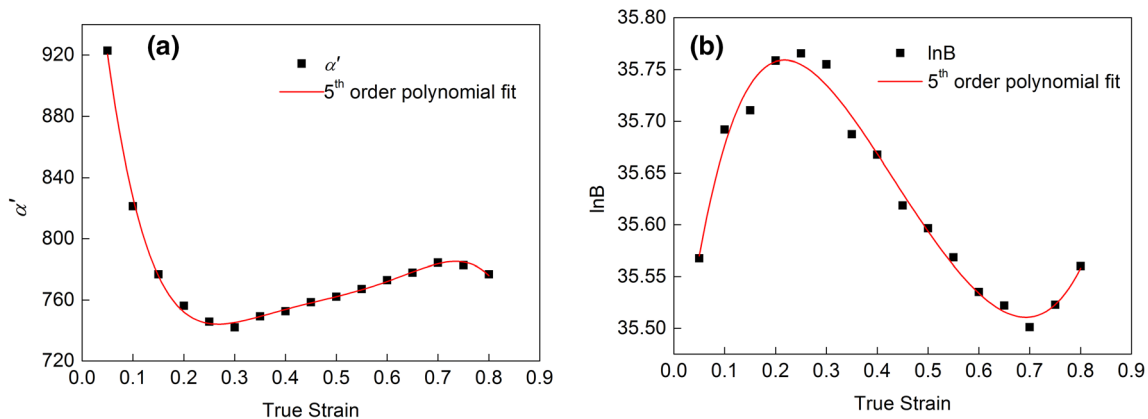
Fig. 4 Relationships between α' (a), $\ln B$ (b) and the true strain ε by polynomial fit of the experimental steel

Table 2 Values of the coefficients in Eq. (8)

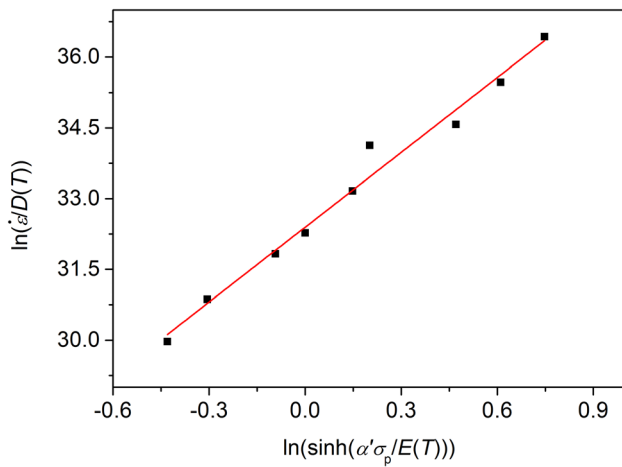| α'_ε	Value	$(\ln B)_\varepsilon$	Value
α'_0	1246.79011	B_0	34.89706
α'_1	− 5780.52269	B_1	12.74835
α'_2	27,975.91242	B_2	− 75.94073
α'_3	− 62,194.42322	B_3	176.16986
α'_4	65,534.35389	B_4	− 185.83702
α'_5	− 26,387.09852	B_5	74.38553

Fig. 5 Relationship between $\ln(\dot{\varepsilon}/D(T))$ and $\ln(\sinh(\alpha'\sigma_p/E(T)))$

$$\sigma = \frac{E(T)}{\alpha'_\varepsilon}\arcsin h\left[\exp\left(\frac{\ln[\dot{\varepsilon}/D(T)] - (\ln B')_\varepsilon}{n'_\varepsilon}\right)\right] \quad (13)$$

3.2 Apparent Arrhenius constitutive model

The traditional Arrhenius hyperbolic sine constitutive model was also established in this work in order to have a comparative analysis. The calculation method of the model is very mature, which can be referred to some literatures [14, 22, 28, 29], so it would not be described in detail here. The relationship between $\ln[\sinh(\alpha\sigma_p)]$ and $\ln Z$ of the experimental steel is shown in Fig. 7. The Arrhenius constitutive equation based on peak stress can be obtained as:

$$\begin{aligned}Z &= \dot{\varepsilon}\exp(309583/(RT)) \\ &= 8.17834 \times 10^{10}(\sinh(0.01\sigma_p))^{5.16}\end{aligned} \quad (14)$$

Strain-compensated Arrhenius hyperbolic sine constitutive model was also established. The relationship between the material constants α, n, $\ln A$, Q and ε was fitted by a 5th order polynomial as shown in Fig. 8 and Eq. (15).

The coefficients of the 5th order polynomial are shown in Table 4.

$$\begin{aligned}\alpha_\varepsilon &= \alpha_{0+}\alpha_1\varepsilon + \alpha_2\varepsilon^2 + \alpha_3\varepsilon^3 + \alpha_4\varepsilon^4 + \alpha_5\varepsilon^5 \\ n_\varepsilon &= N_{0+}N_1\varepsilon_+N_2\varepsilon^2 + N_3\varepsilon^3 + N_4\varepsilon^4 + N_5\varepsilon^5 \\ (\ln A)_\varepsilon &= A_0 + A_1\varepsilon_+A_2\varepsilon^2 + A_3\varepsilon^3 + A_4\varepsilon^4 + A_5\varepsilon^5 \\ Q_\varepsilon &= Q_0 + Q_1\varepsilon + Q_2\varepsilon^2 + Q_3\varepsilon^3 + Q_4\varepsilon^4 + Q_5\varepsilon^5\end{aligned} \quad (15)$$

By substituting the coefficients listed in Eq. (15) and Table 4 into Eq. (1), the strain-compensated Arrhenius model can be obtained:

$$\sigma = \frac{1}{\alpha_\varepsilon}\arcsin h\left[\exp\left(\frac{Q_\varepsilon/RT + \ln\dot{\varepsilon} - (\ln A)_\varepsilon}{n_\varepsilon}\right)\right] \quad (16)$$

3.3 Comparison of the constitutive models

In order to verify the constitutive models, the experimental results were compared with the predicted results as shown in Fig. 9. From Fig. 9, it can be found that the predicted values of the physical constitutive model with exponent n' and the traditional Arrhenius constitutive model agree well with the experimental values under all deformation conditions. But the physical constitutive model with exponent 5 does not have good accuracy to predict the behavior of flow stress, specifically at lower strain rates (0.01 s^{-1} and 0.1 s^{-1}).

This may be because that when the stress exponent in the physical constitutive model is 5, it means that the deformation mechanism of the material at this time is slip and climb of dislocations, so the only softening mechanism considered is dynamic recovery (DRV) [17, 19, 20, 30]. At lower strain rates (0.01 s^{-1} and 0.1 s^{-1}), the hot deformation flow stress curves exhibit typical DRX type, the DRX process eliminates the deformation defects such as dislocations and subgrain boundaries in the deformed matrix through the nucleation and growth of DRX grains, and this process is realized by the migration of large-angle
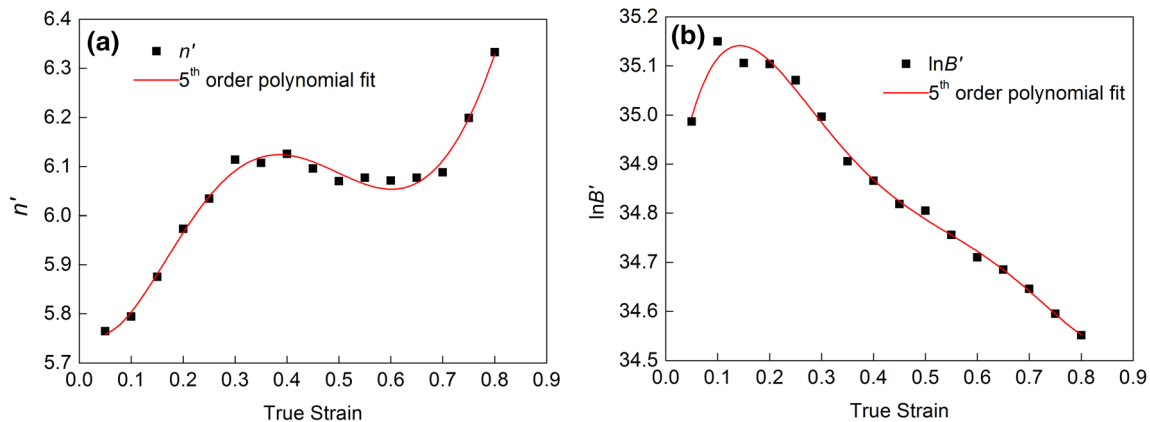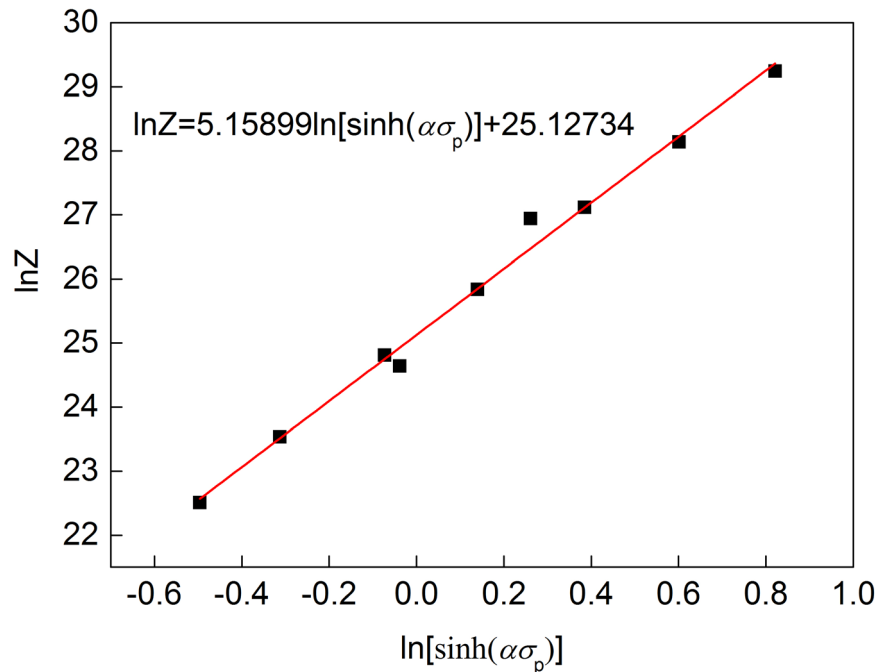

Fig. 6 Relationships between n' (a), $\ln B'$ (b) and the true strain ε by polynomial fit of the experimental steel

Table 3 Values of the coefficients in Eq. (12)

n'_ε	Value	$(\ln B')_\varepsilon$	Value
N'_0	5.03092	B'_0	34.69423
N'_1	4.19023	B'_1	13.71976
N'_2	− 21.03615	B'_2	− 85.20482
N'_3	40.18125	B'_3	208.35833
N'_4	− 38.00074	B'_4	− 226.72587
N'_5	15.23369	B'_5	91.57615

Fig. 7 Relationship between $\ln[\sinh(\alpha\sigma_p)]$ and $\ln Z$

$$\ln Z = 5.15899\ln[\sinh(\alpha\sigma_p)] + 25.12734$$

grain boundaries . As a result, the DRX softening is somehow affecting the stress values, and this could lead to a significant error of the model. When the strain rate increases to 1 s^{-1}, it can be seen that the error has reduced. At higher strain rates (10 s^{-1} and 30 s^{-1}) when DRX is not likely to occur and the only softening mechanism is DRV, deformation mechanism of the material at this time is slip and climb of dislocations, which is suitable for the physical constitutive equation with exponent 5, so the predicted values are in good agreement with the experimental values.

In addition, the calculated values of n' in the physical constitutive equation are obviously bigger than 5 (n' value calculated is 5.29 based on peak stress and n' values range from 5.7 to 6.8 under different strains), indicating that there may be other deformation mechanisms in addition to dislocation slip and climb under the experimental conditions in this paper. Zhao et al. [31, 32] found that there were two

different mechanisms of vanadium microalloyed steel under different deformation conditions, namely dislocation climb and dislocation cross slip. In the general form of the physical constitutive model, variable stress exponent n' replaces 5 and all deformation mechanisms are considered comprehensively, so the predicted values agree well with the experimental values under all deformation conditions.

In order to further verify the prediction accuracy of the proposed constitutive models, the correlation coefficient R and average absolute relative error δ are also used in this work, as shown in Eq. (17)–(18) [33, 34].

$$R = \frac{\sum_{i=1}^{N}(E_i - \overline{E})(P_i - \overline{P})}{\sqrt{\sum_{i=1}^{N}(E_i - \overline{E})^2(P_i - \overline{P})^2}} \qquad (17)$$
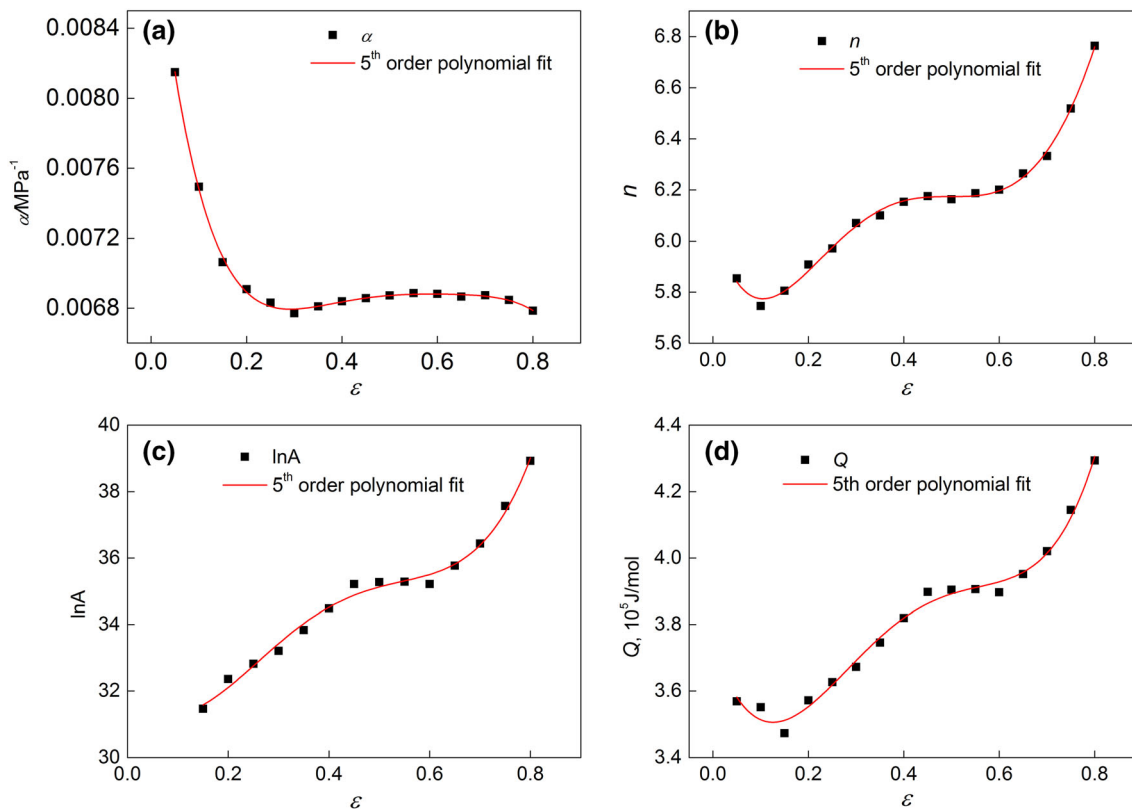
Fig. 8 Relationships between α (**a**), n (**b**), lnA (**c**), Q (**d**) and the true strain ε by polynomial fit

Table 4 Values of the coefficients in Eq. (15)

| α_ε		n_ε		$(\ln A)_\varepsilon$		$Q_\varepsilon/$ (J mol^{-1})	
α_0	0.0092	N_0	6.0682	A_0	32.3926	Q_0	3.7433×10^5
α_1	-0.0262	N_1	-6.6472	A_1	-25.4354	Q_1	-4.3666×10^5
α_2	0.1072	N_2	47.7776	A_2	180.8453	Q_2	2.4768×10^6
α_3	-0.2094	N_3	-118.4639	A_3	-348.6561	Q_3	-4.3361×10^6
α_4	0.1988	N_4	121.6593	A_4	224.8116	Q_4	2.4243×10^6
α_5	-0.0743	N_5	-41.9518	A_5	-7.1398	Q_5	1.4497×10^5

$$\delta = \frac{1}{N} \sum_{i=1}^{N} \left| \frac{E_i - P_i}{E_i} \right| \tag{18}$$

where E_i is the experimental value of flow stress, P_i is the predicted value, $\overline{E}$ is the average value of E_i, $\overline{P}$ is the average value of P_i, N is the number of data points for analysis ($N = 400$).

Figure 10 shows the linear correlation between the experimental values and the predicted values calculated by the constitutive models. It is clearly seen that most of the data points lie very close to the line. The R value of the physical constitutive model with exponent 5 is 0.990, and

the δ value is 10.54%. So the model has lower accuracy than the physical constitutive model with exponent n', of which the R value is 0.992 and the δ value is 3.83%. The R value of the traditional Arrhenius constitutive model is 0.991, and the δ value is 4.58%. So, the accuracy of the physical constitutive model with exponent n' is the highest.

From analysis above, it is concluded that the general form of the physical constitutive model with exponent n' has the highest accuracy, and the accuracy is even higher than that of the traditional Arrhenius constitutive model, thus can be used to accurately predict the flow stress curves of the experimental steel. Therefore, a new model is
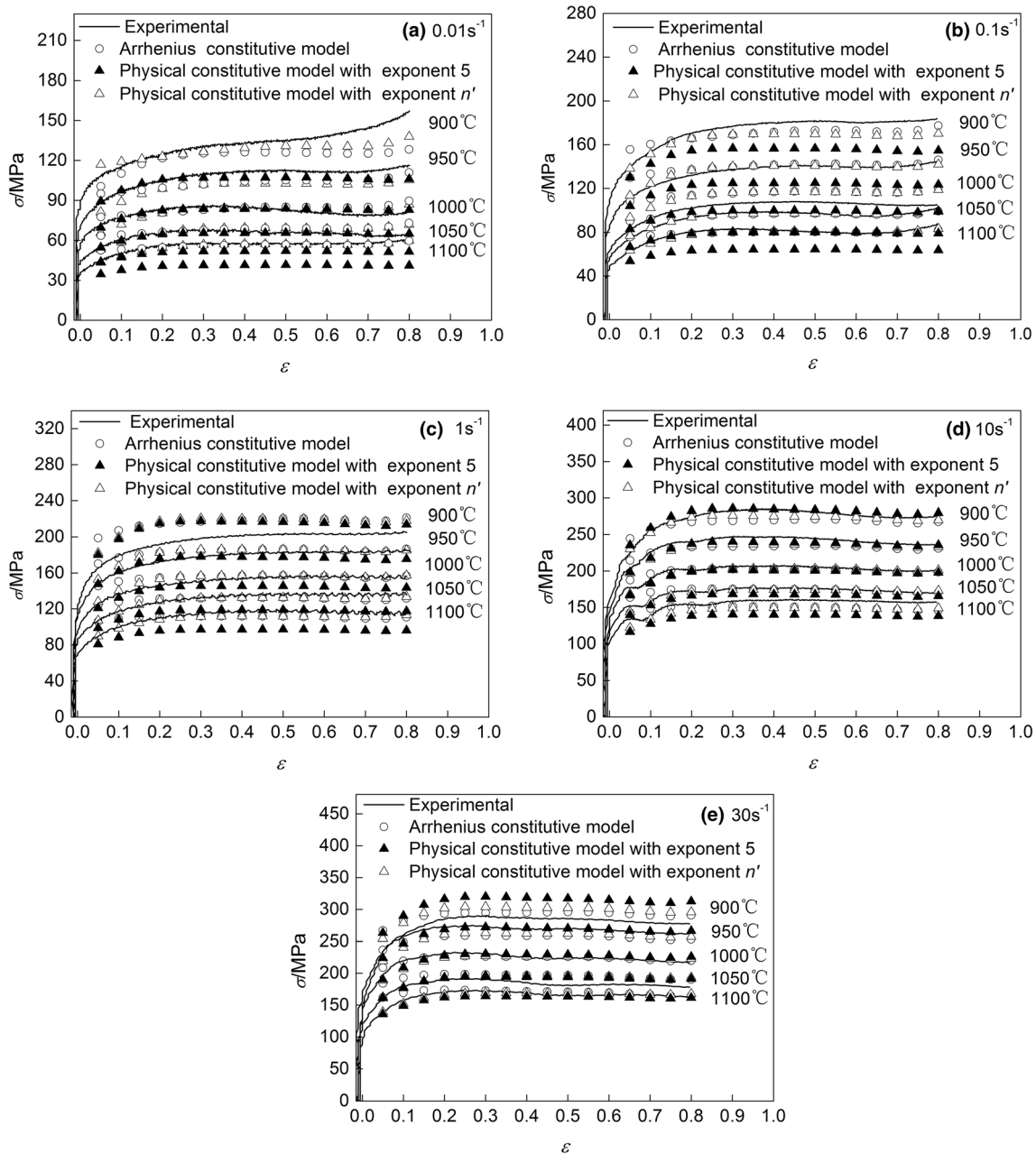
Fig. 9 Comparisons between predicted and measured flow stress curves of the experimental steel under different deformation conditions

proposed and verified in this work to predict flow stress of Nb–Ti microalloyed C–Mn–Al high strength steel, which is not only simple and effective, but also has certain physical and metallurgical backgrounds.

4 Conclusions

1. Considering the influence of temperature on Young's modulus (E) and austenite self-diffusion coefficient (D), the physical constitutive equations of the experimental steel based on peak stress are established as $\dot{\varepsilon} \exp\left(\frac{270000}{RT}\right) = 1.32 \times 10^{14} \left[\sinh\left(\frac{1055.836 \times \sigma_p}{E(T)}\right)\right]^5$ and $\dot{\varepsilon} \exp\left(\frac{270000}{RT}\right) = 1.17 \times 10^{14} \left[\sinh\left(\frac{1055.836 \times \sigma_p}{E(T)}\right)\right]^{5.29}$.

2. The correlation coefficient R of the physical constitutive model with exponent 5 is 0.990, and the average absolute relative error δ is 10.54%. The physical constitutive model with exponent n' has higher accuracy, the correlation coefficient R of which is 0.992, and the average absolute relative error δ is 3.83%.
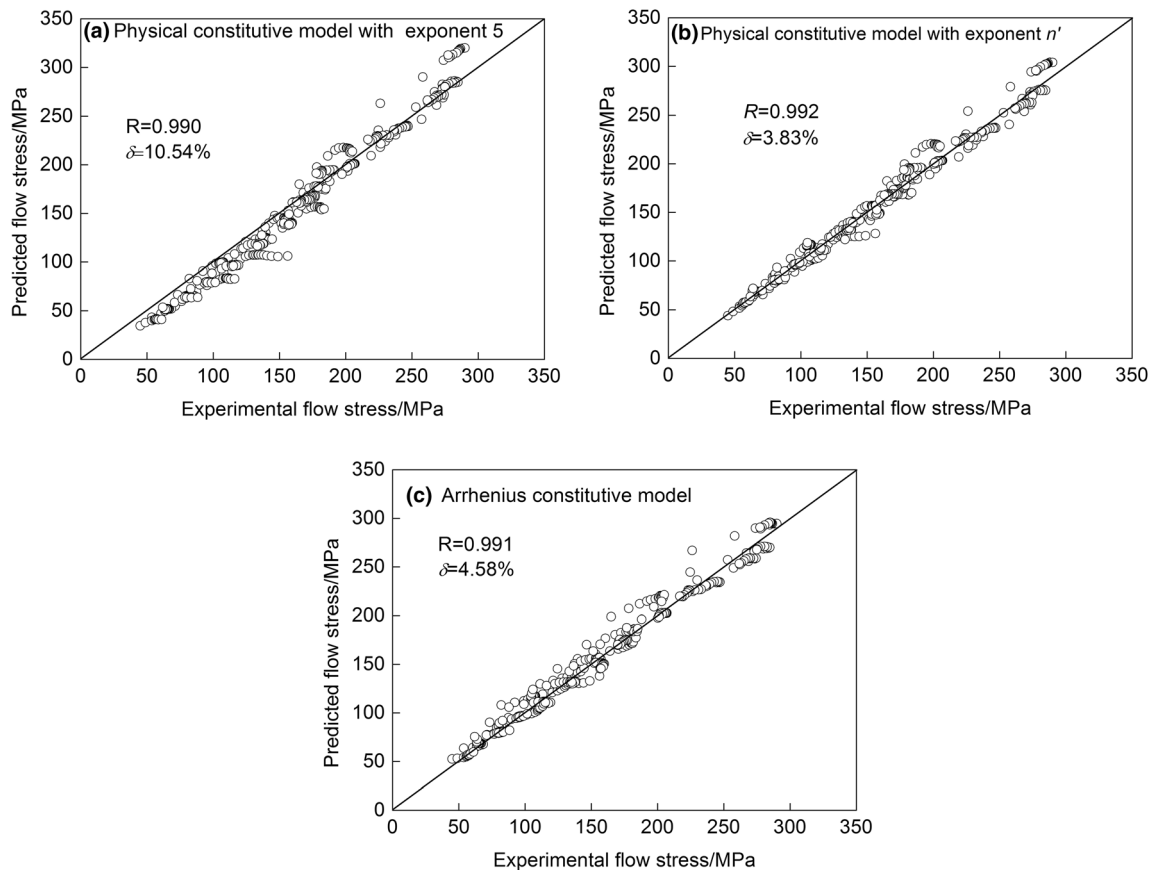
Fig. 10 Correlation between the experimental and predicted flow stress data from the constitutive models

3. The correlation coefficient R of the traditional Arrhenius constitutive model is 0.991, and the average absolute relative error δ is 4.58%. The accuracy of the physical constitutive model with exponent n' is higher than that of the traditional Arrhenius constitutive model, thus can be an alternative way to predict the flow curves of steels, which is not only effective and simple, but also has physical and metallurgical backgrounds.

References

1. Pan H B, Yan J and Liu Y G, Heat Treat Met **41** (2016) 101.
2. Fu B, Yang W Y, Li L F and Sun Z, Acta Metall Sin **49** (2013) 408.
3. Emo J, Maugis P and Perlade A, Comput Mater Sci **125** (2016) 206.
4. El-Sherbiny A, El-Fawkhry M K, Shash A Y and Hossany T, J Mater Res Technol **9** (2020) 3578.
5. Deng Y G, Di H S and Misra R D K, J Mater Res Technol **9** (2020) 14401.
6. Jo M C, Jo M C, Zargaran A, Sohn S S, Kim N J, and Lee S, Mater Sci Eng A **806** (2021) 140823.
7. Zeng Z, Reddy K M, Song S, Wang J, Wang L, and Wang X, Mater Charact **164** (2020) 110324.
8. Kaar S, Krizan D, Schwabe J, Hofmann H, Hebesberger T, Commenda C, and Samek L, Mater Sci Eng A **735** (2018) 475.
9. Soleimani M, Kalhor A and Mirzadeh H, Mater Sci Eng A **795** (2020) 140023.
10. Li Z C, Ding H and Cai Z H, Mater Sci Eng A **639** (2015) 559.
11. Kang J, Li Y J, Wang X H, Wang H S, Yuan G, Misra R D K, and Wang G D, Mater Sci Eng A **742** (2019) 464.
12. Wang T, Hu J and Misra R D K, Mater Sci Eng A **753** (2019) 99.
13. Zhang Y, Li X, Wei K, Wan Z, Jia C, Wang T, and Liang H, Acta Metall Sin **56** (2020) 1401.
14. Zhao M, Qin S, Feng J, Dai Y, and Guo D, Acta Metall Sin **56** (2020) 960.
15. Ramana A V, Balasundar I, Davidson M J, Balamuralikrishnan R, and Raghu T, Trans Indian Inst Met **72** (2019) 2869.
16. Gao Z H, Cai Q W, Xie B S, Chen X, Xu L X, and Yun Y, Trans Indian Inst Met **72** (2019) 2793.
17. Cabrera J M, Al Omar A, Prado J M, and Jonas J J, Metall Mater Trans A **28** (1997) 2233.

18. Cabrera J M, Ponce J and Prado J M, J Mater Process Technol **143** (2003) 403.

19. Cabrera J M, Jonas J J and Prado J M, Mater Sci Tech **12** (1996) 579.

20. Mirzadeh H, Cabrera J M and Najafizadeh A, Acta Mater **59** (2011) 6441.

21. El Wahabi M, Cabrera J M and Prado J M, Mater Sci Eng A **343** (2003) 116.

22. Wei H L, Liu G Q, Xiao X and Zhang M H, Acta Metall Sin **49** (2013) 731.

23. Wei H L, Liu G Q and Zhang M H, Mater Sci Eng A **602** (2014) 127.

24. Ren S J, Wang K L and Lu S Q, Chin J Nonferrous Met **30** (2020) 1289.

25. Liu J J, Wang K L and Lu S Q, Chin J Nonferrous Met **30** (2020) 1611.

26. Feng R, Wang K L and Lu S Q, Rare Met Mater Eng **50** (2021) 525.

27. Frost H J, Ashby M F, Deformation-mechanism maps: the plasticity and creep of metals and ceramics. Oxford: Pergamon Press; 1982.

28. Chen L L, Luo R, Yang Y T, Peng C T, Gui X, Zhang J, Song K Y, Gao P and Cheng X N, Trans Indian Inst Met **72** (2019) 2997.

29. Neethu N, Hassan N A, Kumar R R, Chakravarthy P, Srinivasan A, and Rijas A M, Trans Indian Inst Met **73** (2020) 1619.

30. Cabrera J M and Prado J M, Adv Technol Mater Mater Process J **4** (2002) 45.

31. Zhao H T, Liu G Q and Xu L, Mater Sci Eng A **559** (2013) 262.

32. Zhao H T, Qi J and Liu G Q, J Mater Res Technol **9** (2020)11319.

33. El-Atya A A, Xu Y and Ha S, Mater Sci Eng A **731** (2018) 583.

34. Rasaee S and Mirzaei A H, Trans Indian Inst Met **72** (2019) 1023.